Journal Pre-proof

Paraspinal Myopathy-Induced Intervertebral Disc Degeneration and Thoracolumbar Kyphosis in TSC1mKO Mice Model – A Preliminary Study

Hwee Weng Dennis HEY MBBS, MRCS, MMed (Orth), MCI, FRCSEd (Orth) ,
Wing Moon Raymond LAM Ph.D. ,
Chloe Xiaoyun CHAN MBBS (Spore), MRCS (Ire) ,
Wen-Hai ZHUO M.D. ,   Elisa Marie CROMBIE Ph.D. ,
Tuan Chun TAN Ph.D. ,   Way Cherng CHEN Ph.D. ,
Simon COOL Ph.D. ,   Shih Yin TSAI Ph.D.

Please cite this article as: Hwee Weng Dennis HEY MBBS, MRCS, MMed (Orth), MCI, FRCSEd (Orth) , Wing Moon Raymond LAM Ph.D. ,   Chloe Xiaoyun CHAN MBBS (Spore), MRCS (Ire) , Wen-Hai ZHUO M.D. ,   Elisa Marie CROMBIE Ph.D. ,   Tuan Chun TAN Ph.D. , Way Cherng CHEN Ph.D. ,   Simon COOL Ph.D. ,   Shih Yin TSAI Ph.D. ,   Paraspinal Myopathy-Induced Intervertebral Disc Degeneration and Thoracolumbar Kyphosis in TSC1mKO Mice Model – A Preliminary Study, *The Spine Journal* (2021), doi: https://doi.org/10.1016/j.spinee.2021.09.003

This is a PDF file of an article that has undergone enhancements after acceptance, such as the addition of a cover page and metadata, and formatting for readability, but it is not yet the definitive version of record. This version will undergo additional copyediting, typesetting and review before it is published in its final form, but we are providing this version to give early visibility of the article. Please note that, during the production process, errors may be discovered which could affect the content, and all legal disclaimers that apply to the journal pertain.

- TSC1 gene knockout in a mouse resulted in paraspinal muscle myopathy.

- TSC1mKO mice is by far, the best model to study the pathological consequence of sarcopenia.

- Paraspinal muscle myopathy was established as early as 9 months.

- TSC1mKO mice developed disc degeneration and disc wedging at 9 months.

- Kyphosis of the spine with disc height loss and vertebral body wedging followed.

Paraspinal Myopathy-Induced Intervertebral Disc Degeneration and Thoracolumbar Kyphosis in TSC1mKO Mice Model – A Preliminary Study

First author

Hwee Weng Dennis <u>HEY</u> [a]

MBBS, MRCS, MMed (Orth), MCI, FRCSEd (Orth)

[a] University Orthopaedics, Hand and Reconstructive Microsurgery Cluster (UOHC)

National University Health System (NUHS) [SEP]

5 Lower Kent Ridge Rd, Singapore 119074

doshhwd@nus.edu.sg

Joint First Author:

Wing Moon Raymond <u>LAM</u> [b]

Ph.D.

[b] National University of Singapore Engineering Programme (NUSTEP)

Department of Orthopedic Surgery, Yong Loo Lin School of Medicine

National University of Singapore (NUS) [SEP]

10 Medical Dr, Singapore 117597

doslwmr@nus.edu.sg

Co-authors

Chloe Xiaoyun <u>CHAN</u>

MBBS (Spore), MRCS (Ire)

[a] University Orthopaedics, Hand and Reconstructive Microsurgery Cluster (UOHC)

National University Health System (NUHS)

5 Lower Kent Ridge Rd, Singapore 119074

chloe_xiaoyun_chan@nuhs.edu.sg

Wen-Hai <u>ZHUO</u> [b]

M.D.

[b] Department of Orthopedic Surgery, Yong Loo Lin School of Medicine

National University of Singapore (NUS)

10 Medical Dr, Singapore 117597

Elisa Marie CROMBIE [c]

Ph.D.

[c] Department of Physiology, Yong Loo Lin School of Medicine

National University of Singapore (NUS)

10 Medical Dr, Singapore 117597

e0238017@u.nus.edu

Tuan Chun TAN [d]

Ph.D.

[d] Institute of Medical Biology (IMB)

Agency for Science, Technology and Research (A*STAR)

8a Biomedical Grove, Singapore 138648

Tuanchun.tan@imb.a-star.edu.sg

Way Cherng CHEN [e]

Ph.D.

[e] Bruker Singapore Pte Ltd, Singapore

30 Biopolis St, Singapore 138671

Way_Cherng.Chen@bruker.com

Simon COOL [d]

Ph.D.

[d] Institute of Medical Biology (IMB)

Agency for Science, Technology and Research (A*STAR)

8a Biomedical Grove, Singapore 138648

simon.cool@imb.a-star.edu.sg

Shih Yin TSAI [c]

Ph.D.

[c] Department of Physiology, Yong Loo Lin School of Medicine

National University of Singapore (NUS)

10 Medical Dr, Singapore 117597

phsts@nus.edu.sg

Corresponding author

Hwee Weng Dennis HEY

MBBS, MRCS, MMed (Orth), MCI, FRCSEd (Orth)

[a] University Orthopaedics, Hand and Reconstructive Microsurgery Cluster (UOHC)

National University Health System (NUHS) SEP

5 Lower Kent Ridge Rd, Singapore 119074

doshhwd@nus.edu.sg

ABSTRACT:

Background. Increasing kyphosis of the spine in a human is a well-recognized clinical phenomenon that has been associated with back pain, poor physical performance and disability. The pathophysiology of age-related kyphosis is complex and has been associated with physiological changes in vertebrae, intervertebral disc (IVD) and paraspinal musculature, which current cross-sectional studies are unable to demonstrate. Creating an *in vivo*, paraspinal myopathic animal model for longitudinal study of these changes under controlled conditions is thus warranted.

Purpose. To confirm the TSC1 *gene* knockout effect on paraspinal muscle musculature; to analyze the development of spinal kyphosis, IVD degeneration and vertebra structural changes in a longitudinal manner to gain insights into the relationship between these processes.

Study design. A prospective cohort study of 28 female mice, divided into 4 groups – 9-months-old TSC1mKO (n=7), 9-months-old control (n=4),12-months-old TSC1mKO (n=8) and 12-months-old controls (n=9).

alignment (Cobb's angle), vertebral height, vertebral body wedging, disc height index (DHI), disc wedge index (DWI), histomorphometry of trabecular bone and erector spinae muscle cross-sectional area. Paraspinal muscle specimens were harvested to assess for myopathic features with H&E stain, muscle fiber size, density of triangular fiber and central nucleus with WGA/DAPI stain, and percentage of fibers with PGC-1α stain. Intervertebral discs were evaluated for disc score using FAST stain.

Results. Compared to controls, paraspinal muscle sections revealed features of myopathy in TSC1mKO mice similar to human sarcopenic paraspinal muscle. While there was significantly greater presence of small triangular fiber and density of central nucleus in 9-and 12-months-old TSC1mKO mice, significantly larger muscle fibers and decreased erector spinae muscle cross-sectional area were only found in 12-months-old TSC1mKO mice compared to controls. TSC1mKO mice developed accelerated thoracolumbar kyphosis, with significantly larger Cobb angles found only at 12 months old. Structural changes to the trabecular bone in terms of higher bone volume fraction and quality, as well as vertebral body wedging were observed only in 12-months-old TSC1mKO mice when compared to controls. Disc degeneration was observed as early as 9 months in TSC1mKO mice and corresponded with disc wedging. However, significant disc height loss was only observed when comparing 12-months-old TSC1mKO mice with controls.

Conclusions. This study successfully shows the TSC1 gene knockout effect on the development of paraspinal muscle myopathy in a mouse which is characteristic of sarcopenia. The TSC1mKO mice is by far the best model available to study the pathological consequence of sarcopenia on mice spine. With paraspinal muscle myopathy established as early as 9 months, TSC1mKO mice developed disc degeneration and disc wedging. This is followed by kyphosis of the spine at 12 months with concomitant disc height loss and vertebral body wedging due to bone remodeling. Age-related bone loss was not found in our study, suggesting osteoporosis and myopathy-induced vertebral body wedging are likely two independent processes.

Clinical significance. This is the first study to provide key insights on the early and late consequences of paraspinal myopathy on intervertebral disc degeneration, spinal kyphosis, and vertebral body changes. With this new understanding, future studies evaluating therapies for spinal degeneration may be performed to develop time-sensitive interventions.

Keywords: Intervertebral Disc Degeneration; Kyphosis; Micro-CT; Paraspinal Muscle; Sarcopenia; Spinal Loading; TSC1mKO

5

Level of Evidence: NA

Abbreviations

AF: annulus fibrosus

BV/TV: bone volume fraction

DAPI: 4',6-Diamidino-2-Phenylindole

DHI: disc height index

DWI: disc wedge index

FAST: Fast green, Alcian blue, Safranin-O, and Tartrazine

H&E: haematoxylin and eosin

IHC: immunohistochemical

IVD: intervertebral disc

Micro-CT: Micro-computed tomography

mTORC1: mammalian target of rapamycin complex 1

NP: nucleus pulposus

PGC-1α: Peroxisome proliferator-activated receptor γ coactivator 1α

Tb.Th.: trabecular thickness

Tb.N.: trabecular number

Tb.Sp.: trabecular separation

TSC1: tuberous sclerosis complex 1

WGA: wheat germ agglutinin

The kyphosing process of the spine in a human is a well-recognized clinical phenomenon (1) that has been associated with back pain, poor physical performance and disability. The incidence of patients with spinal hyperkyphosis above 70 years of age has been reported to be up to 40% (2), and in its most severe form, can compromise pulmonary and neurovascular function leading to mortality (3). The pathophysiology of spinal kyphosis is complex, and has been associated with changes in vertebrae (4), intervertebral disc (5), and paraspinal musculature (6). Current studies evaluating this process are largely cross-sectional and are not useful in determining cause-effect relationships among these factors (7-12). To elucidate the pathological consequence of paraspinal myopathy, deemed in recent studies as an integral component of age-related spinal kyphosis, obtaining an *in vivo* animal model for longitudinal study under controlled conditions is warranted.

The occurrence of spinal kyphosis had been demonstrated in murine models with muscle dysfunction such as in the Duchenne muscular dystrophy (mdx) mouse model (13) and $Bub1b^{+/GTTA}$ progeroid mouse model (14), suggesting the possibility of muscle wasting as its cause (15, 16). However, due to the multiple confounding systemic effects resulting from genetic modifications in these mouse models, an exact cause-effect relationship between muscle weakness and spinal kyphosis cannot be confirmed. Other existing chronic paraspinal muscle injury mice models demonstrating spinal kyphosis development (17) suffers from limitations due to the use of surgical detachment and ligation of paraspinal muscle to induce muscle dysfunction – methods that do not mimic paraspinal myopathy secondary to aging. In order to isolate and push forth investigations examining the effects of age-related myopathy on spinal alignment, a tissue-specific, genetically-modified mouse model that gives a slow and progressive onset of myopathy would be favorable.

The mammalian target of rapamycin complex 1 (mTORC1) with negative feedback by tuberous sclerosis complex 1 (TSC1), is a protein complex that regulates various anabolic cellular processes in muscle (18). Sustained activation of mTORC1 leads to a blockade in autophagy and increase in oxidative stress – mechanisms that are implicated for the development of age-related sarcopenia in human (19, 20). The TSC1mKO mouse, in which *Tsc1 (inhibitor)* was deleted only in muscle tissue, demonstrated chronic signaling of mTORC1 in muscle tissue resulting in late-onset myopathy with gradual muscle dysfunction – a feature of sarcopenia (21), hence this model is most suitable to investigate the effects of age-related myopathy for future clinical translation and extrapolation.

7

myopathy in the limbs, till date, a detailed assessment of paraspinal muscle myopathy in TSC1mKO mice has yet to be performed. Its role in spinal kyphosis development, as well as association with other known confounders for age-related changes of the spine – intervertebral disc (IVD) degeneration and vertebral bone structural changes, remain undetermined. In this study using TSC1mKO mice, we aimed to 1) confirm the effect of TSC1 gene knockout on paraspinal muscle musculature, and 2) trend the development of spinal kyphosis, intervertebral disc (IVD) degeneration and vertebral bone structural changes in a longitudinal manner to gain further insights into the relationships between these processes.

Animal subjects

TSC1mKO mice were generated by breeding TSC1 flox mice (contains Lox sequence) with Ckmm-Cre mice (contains Cre sequence) purchased from Jackson laboratory (22). Cre-Lox recombinase technology allows site-specific DNA deletions of specific cell types. Therefore, Ckmm-Cre mice, with Ckmm-Cre expression in its muscle, allowed skeletal and cardiac muscle-specific deletion of the *Tsc1* gene, hence producing TSC1mKO mice with isolated myopathy. TSC1 flox littermates without Ckmm-Cre transgene were used as age-matched control mice. All mice included were females for standardization. Mice tail tips were harvested for genotyping, which was performed by PCR according to JAX lab protocol (23, 24).

All mice were housed with free access to food and water. Mice were euthanized by decapitation at the age of 9-months (control, n=4 and TSC1mKO, n=7) or 12-months (control, n=9 and TSC1mKO, n=8) respectively. All procedures were performed in accordance with the National University of Singapore's Institutional Animal Care and Use Committee (IACUC) guidelines for animal experiments (R17-0195).

Micro-computed tomography (micro-CT) analysis

After the mice were sacrificed, scans of the thoracic and lumbar spine were performed at 18 μm pixel size cuts by SkyScan 1176 micro-CT (Bruker, Kontich, Belgium), equipped with a 0.5mm aluminium filter at 50kV and current of 500 μA. 2D axial views were reconstructed using the provided NRecon software. Sagittal views were subsequently reconstructed using DataViewer (Bruker) from the corresponding 2D axial images. From the reconstructed sagittal images, sagittal spinal alignment was measured using the Cobb method with ImageJ software (NIH, 1.53). The values derived by two blinded and independent orthopedic surgeons were averaged.

Axial cross-sectional area of the erector spinae muscle at the level of L4 was measured using the ROI contour tool on ImageJ.

The vertebral height, vertebral body wedging, histomorphometry of trabecular bone, disc height and disc wedge indexes in the region of the lumbar spine (L1 to L6) were analyzed using CTAn software (1.15.4) supplied with the SkyScan 1176. Given that the thoracic and lumbar vertebrae are structurally (25) and biomechanically different (26), the lumbar region (L1 to L6) was chosen for analysis in this study for consistency. Vertebral body wedging was calculated as the ratio

9

manually by region of interest, with the aid of interpolation tools in the coronal plane of each lumbar vertebra (L1 to L6). Microstructural parameters including bone volume fraction (BV/TV, %), trabecular thickness (Tb.Th., μm), trabecular number (Tb.N., mm^{-1}), and trabecular separation (Tb.Sp., μm) were calculated by CTAn. Coronal sections of the L4 vertebral body were captured to demonstrate gross differences in bone volume fraction.

Disc Height Index (DHI) is the thickness of the IVD relative to the vertebra height, and was determined by the following equation: Disc Height Index (DHI) = $[2 \times (DH1 + DH2 + DH3)]/(A1 + A2 + A3 + B1 + B2 + B3)$(27, 28). A and B represent the height of the vertebral bone immediately rostral and caudal to the IVD of interest, respectively; and DH represents the disc height between the two adjacent vertebrae (A and B) (Figure 1). The disc wedge index (DWI) reflects the shape of the IVD, and was calculated by dividing DH3/DH1 (27, 28) (Figure 1).

Histology and immunohistochemical (IHC) staining

After micro-CT scans, paraspinal muscle at the level of L4 was harvested and fixed with 4% paraformaldehyde for 5 days. This was followed by gradient ethanol dehydration, xylene clearance and paraffin embedment before slicing into 5μm cross-sections. Muscle sections were stained by Mayer haematoxylin and eosin (H&E) stain to analyze degree of myopathy. The choice of muscle sampling at L4 was to demonstrate proof of concept of TSC1mKO mice in generating myopathy that would be minimally confounded by the effects of progressive spinal kyphosis.

For immunohistochemical (IHC) staining, antigen was retrieved using citric acid buffer (pH 6, at 95°C) for 10 mins. Muscle sections were treated with protein block (Abcam 156024) for 10 minutes followed by overnight incubation at 4°C with primary antibodies (Peroxisome proliferator-activated receptor γ coactivator 1α (PGC-1α) Invitrogen 38021 1:200). After washing with PBS + 0.1% Triton X-100, muscle sections were incubated with Alexa Fluor 555 conjugated wheat germ agglutinin (WGA) and secondary antibodies (Sigma Anti-rabbit IGG CF 488 1:1000) at 4°C for 1 hour, then washed and mounted with Slowfade diamond with DAPI (4',6-Diamidino-2-Phenylindole) (Invitrogen™). Muscle fiber size, density of central nucleus, as well as percentage of small triangular muscle fibers and PGC-1α stained fibers were evaluated by ImageJ.

Spine specimens were cut at the level of T12 to separate thoracic and lumbar regions after decalcification with Morse's solution (10% trisodium citrate, 20% formic acid) for three days at 4°C. Specimens were washed with tap water, dehydrated with 70% and 100% ethanol, cleared with xylene, embedded in paraffin, and sliced into 7μm sagittal sections. After dewaxing and

10

Tartrazine) and graded for disc health according to the standard protocol (29). A 14-point disc score was used to calculate changes in nucleus pulposus (NP) structure and cellularity (6 points), annulus fibrosus (AF) structure (6 points), and AF/NP interface (2 points) (30).

Statistical analysis

Continuous variables were reported using means ± standard deviations. Unpaired t-tests were used to compare differences in the degrees of Cobb's angle, vertebral height, vertebral body wedging, BV/TV, Tb.Th., Tb.N., Tb.Sp, DHI, DWI, erector spinae muscle cross-sectional area, muscle fiber size, density of central nucleus, small triangular muscle fibers, PGC-1α positive fibers and disc score between TSC1mKO and control groups across same time points. One-way ANOVA with Tukey's post-hoc tests were used to determine differences of the above variants between different time points (9 months versus 12 months) within each group. All statistical analyses were performed using IBM SPSS v25.0 with statistical significance set at $P < 0.05$ throughout.

The genotype of TSC1mKO and control mice were confirmed by polymerase chain reaction (PCR) (Figure 2a). Histological examination of H&E stained paraspinal muscle sections of 9- and 12-months-old TSC1mKO revealed features of myopathy such as intracellular inclusions, central nuclei and large myonuclei (Figure 2c, 2e). In addition, vacuolated fibers were found in 12-months-old TSC1mKO mice paraspinal muscle that were not present in 9-months-old counterparts. These myopathic features were absent in the age-matched control mice (Figure 2b, 2d), and showed striking similarities to human sarcopenic paraspinal muscle (31).

From micro-CT images, erector spinae muscle cross-sectional area was smaller in 9- and 12-months-old TSC1mKO mice compared to control mice, with statistical significance at 12 months (9-months-old TSC1mKO 66.97 ± 6.80 mm^2 vs Control 72.84 ± 15.80 mm^2, P=0.35; 12-months-old TSC1mKO 48.54 ± 10.20 mm^2 vs Control 65.02 ± 6.85 mm^2, P=0.007), suggesting paraspinal muscle wasting. On the WGA/DAPI stained muscle sections, larger muscle fiber size, presence of small triangular muscle fiber, and greater density of central nuclei indicates muscle degeneration and myopathy. The average fiber sizes of 12-months-old TSC1mKO mice were larger than the age-matched control mice (12-months-old TSC1mKO 2309.41 ± 856.67 μm^2 vs Control 1311.41 ± 79.67 μm^2, P=0.043; Figure 3a-d). The percentage of small triangular muscle fiber was greater in TSC1mKO mice compared to controls, with further increases with age (9-months-old TSC1mKO $4.29 \pm 1.95\%$ vs Control $0.17 \pm 0.21\%$, P<0.001; 12-months-old TSC1mKO $6.30 \pm 4.85\%$ vs Control $0.96 \pm 1.19\%$, P=0.001). Central nucleus densities in 9- and 12-months-old TSC1mKO mice were higher than age matched controls as well (9-months-old TSC1mKO $17.39 \pm 4.95\%$ vs Control $1.02 \pm 0.52\%$, P=0.001; 12-months-old TSC1mKO $18.90 \pm 6.61\%$ vs Control $3.43 \pm 2.19\%$, P=0.021).

In terms of paraspinal muscle immunofluorescence staining, the presence of PGC-1α stained (green fluorescent) fiber suggests muscle degeneration and myopathy. 9-months-old TSC1mKO mice were found to have lower percentage of PGC-1α stained fibers compared to 12-months-old TSC1mKO mice (9-months-old TSC1mKO $14.12 \pm 8.98\%$ vs 12-months-old TSC1mKO $22.94 \pm 3.28\%$, P=0.047), although this only reached borderline significance when compared to age-matched controls (Figure 3e-h).

In terms of spinal alignment, TSC1mKO mice developed accelerated thoracolumbar kyphosis (Figure 4). In comparison with the age-matched control mice, TSC1mKO mice demonstrated a more kyphotic Cobb angle only at 12 months (TSC1mKO $83.67 \pm 17.18°$ vs Control $47.80 \pm 23.48°$, P=0.002). There is also an increase in kyphotic angle observed in TSC1mKO mice from 9

months to 12 months (9-months-old 35.12 ± vs 12-months-old 55.51 ± 24.56°, P=0.009,
Figure 4b), but not in control mice (9-months-old 41.83 ± 15.34° vs 12-months-old 47.80 ±
23.48°, P=0.316).

In terms of bone changes, representative coronal sections of the L4 vertebral body showed higher
bone volume fraction in TSC1mKO mice compared to controls (Figure 5a). At 9 months old, the
differences in trabecular histomorphometry parameters between TSC1mKO and control mice did
not reach statistical significance (Table 1). At 12 months old, TSC1mKO mice had higher bone
volume fraction and quality (higher trabecular number, thickness and lower trabecular separation)
than control mice, albeit without significant loss of vertebral body height (Table 1). In addition,
micro-CT sagittal sections of L1 to L6 vertebrae showed higher bone sclerosis particularly the
anterior aspect of the vertebrae of 12-months-old TSC1mKO mice compared to controls (Figure
5b). TSC1mKO mice generally had a higher vertebral body posterior to anterior ratio (Table 1)
reaching borderline statistical significance, which is suggestive of greater vertebral body wedging
compared to control mice. Vertebral body fractures were not observed in any of the study mice.

In terms of changes in intervertebral disc, more intervertebral disc scores of 12-months-old
TSC1mKO were higher than controls (L1/2, L2/3, L3/4, L4/5, L5/6) compared to 9-month-old
TSC1mKO mice (L1/2, L3/4, L5/6). Qualitative assessment of disc histology showed early signs
of disc degeneration such as reduced extracellular matrix, loss of nucleus pulposus cells and
widened annulus fibrosus lamellae in L5/6 discs of 9-months-old TSC1mKO mice (Figure 6) and
continued to progress at all levels until 12-months-old. The degree of IVD degeneration appeared
to be level-dependent, affecting the lower lumbar levels to a greater extent. At 12 months, the
intervertebral disc at L5/6 had reduction of DHI as well which was not present at 9 months (12-
months-old TSC1mKO 0.081 ± 0.008 vs Control 0.095 ± 0.013, P=0.01; 9-months-old TSC1mKO
0.085 ± 0.009 vs Control 0.082 ± 0.006, P=0.34), and suggests progressive and increasingly rapid
IVD degeneration in TSC1mKO mice only after 9-months-old. In addition to loss of height, DWI
generally increased in TSC1mKO compared to age-matched controls, and was most remarkable at
L2/3 (9-months-old TSC1mKO 1.90 ± 0.17 vs Control 1.58 ± 0.17, P=0.039; 12-months-old
TSC1mKO 2.62 ± 0.60 vs Control 1.80 ± 0.39, P=0.002) and L3/4 levels (9-months-old
TSC1mKO 1.85 ± 0.11 vs Control 1.58 ± 0.07, P=0.014; 12-months-old TSC1mKO 2.39 ± 0.69
vs Control 1.74 ± 0.21, P=0.016) at 9 and 12 months. TSC1mKO mice also showed increase in
DWI at L2/3, L3/4 and L5/6 from 9 to 12 months compared to controls, which showed no changes
in DWI.

TSC1mKO and Control mice.

DISCUSSION

The pathophysiology behind the kyphosing human spine is complex and involves biomorphological changes in paraspinal muscle, vertebral bone and intervertebral disc. Hey et al (32) theorized that the natural inclination of humans to slouch and hunch their spine, served to conserve energy by employing posterior spinal ligamentous tension band in the upright posture, inadvertently contributed to a vicious cycle of underutilization of paraspinal musculature and promotes spinal kyphosis. In conjunction with the aforementioned postural changes, intervertebral disc degeneration leading to loss of disc height, as well as bone remodeling leading to vertebral body wedging further contributed to the development of hyperkyphosis (33, 34). Current studies are inadequate at explaining the exact pathoetiology of this complex physiological process observed in aging. Therefore, this animal study which uses gene knock-out technology to generate tissue-specific myopathy in a rodent model will serve as the first step to produce a model for elucidating the pathological consequence of paraspinal myopathy under controlled conditions. Further studies on bipedal animals will follow to enable bench-to-bedside translation of attained knowledge.

This study had successfully proven the effect of TSC1 gene knockout on the development of paraspinal muscle myopathy in a mouse. Erector spinae muscle cross-sectional area was significantly reduced in 9- and 12-months-old TSC1mkO mice compared to controls, suggesting volumetric loss of paraspinal muscle which may be suggestive of muscle weakness. In an earlier study which employs 12-months-old TSC1mKO mice (21), sarcopenic histological changes such as vacuolated fibers and intracellular inclusions were observed in tibialis anterior muscle. These were also found in the paraspinal muscles of our 9- and 12-months-old TSC1mKO mice on H&E staining. In addition, our study found greater density of small triangular muscle fiber, larger muscle fiber size, and greater density of central nuclei on WGA/DAPI and muscle fibers stained with PGC-1α, which confirmed that TSC1mKO mice develop tissue-specific myopathy that affects both the peripheral and the paraspinal muscles, and can be appropriately used to study the longitudinal effects of myopathy on spinal kyphosis, intervertebral disc degeneration and vertebral bone remodeling. In addition, the slow and progressive onset of myopathy in this model closely mimics the process of sarcopenia – an age-related process marked by gradual muscle dysfunction – making it favorable to be used for understanding the kyphosing process in humans.

14

patients with adult spinal deformity, many recent cross-sectional studies were performed to investigate truncal muscle integrity and its effects on spinal alignment changes in the elderly (35, 36). Lorbergs *et al.* reported that a smaller muscle cross-sectional area and lower quality of thoracic spine muscles were associated with a larger kyphotic Cobb angle in a population aged 50 years and above (35). Several clinical studies have also correlated changes in paraspinal muscle strength with severity of thoracic kyphosis (11, 37). Similar to these observations in humans, Mdx mice (13) and tetranectin-deficient mice (38) with proven muscle weakness have also been shown to develop kyphosis. Our current study uses TSC1mKO mice which displayed consistent reduction of paraspinal muscle quality and kyphosis development in a gradual and age-dependent manner. The changes in Cobb angles at 12-month-old, but not in 9-month-old TSC1mKO mice compared to control counterparts, as well as the significant increase in Cobb angle from 9 to 12-months-old in TSC1mKO mice but not in controls attest to these concepts.

The role of paraspinal myopathy in causing accelerated disc degeneration has been shown in humans, large animals and mice models previously. Increased static compressive stress in intervertebral discs which often occurs when humans assume prolonged energy-conserving slouch postures can result in raised disc pressures (39, 40), thereby inducing disorganized annulus fibers, decreased nuclear cellularity and extracellular aggrecan content (41). This had been demonstrated in an *in vivo* mouse model (42). In large animal studies, injection of botulinum toxin into the paraspinal muscle of monkeys that generated muscle weakness also induced disc degeneration (43). In a literature review, Stokes *et al.* theorized that overloading conditions such as those of impaired neuromuscular control of paraspinal or abdominal muscles can generate tissue trauma and/or adaptive changes resulting in disc degeneration in animal models (44). In our current study, histological analysis following FAST staining confirmed disc degeneration occurring in TSC1mKO mice as early as 9-months-old through reduction of extracellular matrix and cellularity of the nucleus pulposus. Our study also showed greater disc degeneration with widened annulus fibrosus lamellae in aged 12-months-old TSC1mKO mice, with increased severity at the lower lumbar levels. Since the compressive force on the intervertebral discs is more likely experienced in the lower spinal segments due to gravitational force on body weight especially during load-bearing activities, it is expected that these segments manifest the greatest degeneration changes over time.

In addition, notwithstanding that paraspinal myopathy can also cause spinal kyphosis which may be closely related to accelerated disc degeneration, disc wedging, which could contribute to spinal

old, further disc wedging was found in L1/2-L3/4. This was associated with loss of DHI at L5/6 which was significantly lower compared with age-matched controls. The progressive findings of disc wedging and subsequently loss of disc height in aging TSC1mKO mice are possible contributors to increasing spinal kyphosis in a vicious cycle. Based on the chronological sequence of events (Table 4), it is likely that spinal kyphosis occurs early in paraspinal myopathy in association with disc wedging. It is important to highlight that disc wedging may still be reversible in a mobile spine, while loss of disc height is probably not. Therefore, histological disc degenerative changes observed at 9 months may result from dysfunctional loading or mobility mechanics in spinal compression and distraction shown in earlier rabbit studies (45, 46). With persistent kyphosis, continued loading of the spine leads to accelerated disc degeneration which eventually results in irreversible loss of disc height and further spinal kyphosis.

Unlike the mdx mouse model (47), TSC1mKO mice did not show myopathy-induced bone loss. On the contrary, L1-L6 bone volume fraction, trabecular thickness and trabecular number were significantly higher in TSC1mKO mice compared to controls as they reached 12 months of age. According to Wolff's law (40), mechanical loading stimulates bone formation in stressed areas (38, 39), and likely explains why the anterior cortex of vertebral bodies were more sclerotic on micro-CT sagittal cuts. In addition, greater wedging of the lumbar vertebral bodies could be explained by growth modulation following Hueter-Volkmann's law since greater loading exist anteriorly. Therefore, myopathy-induced vertebral body wedging and osteoporosis are likely two independent processes that occurs with aging. The absence of vertebral fractures also ruled out the possibility of fragility fracture as a confounder for spinal kyphosis in the TSC1mKO mice model (48, 49). Nevertheless, bony changes which appeared only at 12 months is likely a delayed process contributing to late-stage spinal kyphosis.

This study is the first to provide key insights on the early and late pathological consequence of paraspinal myopathy on intervertebral disc degeneration, spinal kyphosis, and vertebra changes. While extrapolation of our study findings to humans is discouraged at this stage without further studies on erectus models, this new understanding may potentially form the basis for future studies to look into prevention or reversal of myopathy using various forms of therapies. Prevention and/or reversal of degenerative changes may herald a new paradigm of management strategies in spine surgery.

16

endurance was not directly measured but implicated from the loss of muscle bulk and histological changes mimicking sarcopenic muscles. Future studies can be performed to directly assess paraspinal muscle function via motion analysis and single muscle fiber contractility tests. Secondly, our study included 2 time points (9 and 12 months) to analyze the various spinal components. Having more time points for analysis would allow improved precision in detecting chronological developments of each process. This can be taken into account in future studies. Thirdly, the biomechanics of quadrupedal mice, while reported to be similar to bipedal humans, is not fully identical. Further studies on erectus models such as in monkeys would be required prior to extrapolation of findings to humans.

In summary, this study had successfully proven the effect of TSC1 gene knockout on the development of paraspinal muscle myopathy in a mouse characteristic of human sarcopenia. As such, longitudinal observation of the changes in spinal alignment, intervertebral disc and vertebral body structure may be used to understand spinal changes in human aging. It is by far, the best model available to study the pathological consequence of sarcopenia using a mice spine. With paraspinal muscle myopathy established as early as 9 months, TSC1mKO mice developed disc degeneration and disc wedging. This is followed by kyphosis of the spine with concomitant disc height loss, vertebral body wedging and bone remodeling. Myopathy-induced bone loss was not found in our study, suggesting osteoporosis and myopathy-induced vertebral body wedging are likely two independent processes.

REFERENCES

1.   O. Yaman, S. Dalbayrak, Kyphosis and review of the literature. *Turkish neurosurgery* 24, 455-465 (2014).
2.   D. M. Kado, K. Prenovost, C. Crandall, Narrative review: hyperkyphosis in older persons. *Annals of internal medicine* 147, 330-338 (2007).
3.   D. M. Kado, M. H. Huang, A. S. Karlamangla, E. Barrett-Connor, G. A. Greendale, Hyperkyphotic posture predicts mortality in older community-dwelling men and women: a prospective study. *J Am Geriatr Soc* 52, 1662-1667 (2004).
4.   Y. Wei, W. Tian, G. L. Zhang, Y. W. Lv, G. Y. Cui, Thoracolumbar kyphosis is associated with compressive vertebral fracture in postmenopausal women. *Osteoporos Int* 28, 1925-1929 (2017).
5.   D. M. Kado *et al.*, Factors associated with kyphosis progression in older women: 15 years' experience in the study of osteoporotic fractures. *J Bone Miner Res* 28, 179-187 (2013).
6.   Y. Kasukawa *et al.*, Age-related changes in muscle strength and spinal kyphosis angles in an elderly Japanese population. *Clin Interv Aging* 12, 413-420 (2017).
7.   H. S. Jun *et al.*, The Effect of Lumbar Spinal Muscle on Spinal Sagittal Alignment: Evaluating Muscle Quantity and Quality. *Neurosurgery* 79, 847-855 (2016).
8.   M. Masaki *et al.*, Association of sagittal spinal alignment with thickness and echo intensity of lumbar back muscles in middle-aged and elderly women. *Archives of gerontology and geriatrics* 61, 197-201 (2015).
9.   M. Alpayci *et al.*, Decreased neck muscle strength in patients with the loss of cervical lordosis. *Clinical biomechanics (Bristol, Avon)* 33, 98-102 (2016).
10.   W. Katzman *et al.*, Association of spinal muscle composition and prevalence of hyperkyphosis in healthy community-dwelling older men and women. *The journals of gerontology. Series A, Biological sciences and medical sciences* 67, 191-195 (2012).
11.   A. Mika, V. B. Unnithan, P. Mika, Differences in thoracic kyphosis and in back muscle strength in women with bone loss due to osteoporosis. *Spine* 30, 241-246 (2005).
12.   T. Roghani, M. K. Zavieh, F. D. Manshadi, N. King, W. Katzman, Age-related hyperkyphosis: update of its potential causes and clinical impacts-narrative review. *Aging clinical and experimental research* 29, 567-577 (2017).
13.   N. Laws, A. Hoey, Progression of kyphosis in mdx mice. *Journal of applied physiology (Bethesda, Md. : 1985)* 97, 1970-1977 (2004).

Aging. *Veterinary pathology* 53, 366-389 (2016).

15. S. D. Tyner *et al.*, p53 mutant mice that display early ageing-associated phenotypes. *Nature* 415, 45-53 (2002).

16. M. S. Razzaque, D. Sitara, T. Taguchi, R. St-Arnaud, B. Lanske, Premature aging-like phenotype in fibroblast growth factor 23 null mice is a vitamin D-mediated process. *FASEB journal : official publication of the Federation of American Societies for Experimental Biology* 20, 720-722 (2006).

17. T. G. Cho, S. W. Park, Y. B. Kim, Chronic Paraspinal Muscle Injury Model in Rat. *Journal of Korean Neurosurgical Society* 59, 430-436 (2016).

18. M. Shimobayashi, M. N. Hall, Multiple amino acid sensing inputs to mTORC1. *Cell research* 26, 7-20 (2016).

19. G. A. Joseph *et al.*, Partial Inhibition of mTORC1 in Aged Rats Counteracts the Decline in Muscle Mass and Reverses Molecular Signaling Associated with Sarcopenia. *Molecular and cellular biology* 39 (2019).

20. H. Tang *et al.*, mTORC1 underlies age-related muscle fiber damage and loss by inducing oxidative stress and catabolism. *Aging cell* 18, e12943 (2019).

21. P. Castets *et al.*, Sustained activation of mTORC1 in skeletal muscle inhibits constitutive and starvation-induced autophagy and causes a severe, late-onset myopathy. *Cell metabolism* 17, 731-744 (2013).

22. D. J. Kwiatkowski *et al.*, A mouse model of TSC1 reveals sex-dependent lethality from liver hemangiomas, and up-regulation of p70S6 kinase activity in Tsc1 null cells. *Human molecular genetics* 11, 525-534 (2002).

23. Anonymous (B6.FVB(129S4)-Tg(Ckmm-cre)5Khn/J.

24. Anonymous (Tsc1 flox, Tsc1c.

25. S. H. Tan, E. C. Teo, H. C. Chua, Quantitative three-dimensional anatomy of cervical, thoracic and lumbar vertebrae of Chinese Singaporeans. *Eur Spine J* 13, 137-146 (2004).

26. S. Iyer *et al.*, A biomechanical model for estimating loads on thoracic and lumbar vertebrae. *Clinical biomechanics (Bristol, Avon)* 25, 853-858 (2010).

27. M. Tajerian *et al.*, DNA methylation of SPARC and chronic low back pain. *Mol Pain* 7, 65 (2011).

28. M. Millecamps, M. Tajerian, L. Naso, H. E. Sage, L. S. Stone, Lumbar intervertebral disc degeneration associated with axial and radiating low back pain in ageing SPARC-null mice. *Pain* 153, 1167-1179 (2012).

29. V. Y. Leung, W. C. Chan, S. C. Hung, K. M. Cheung, D. Chan, Matrix remodeling during intervertebral disc growth and degeneration detected by multichromatic FAST staining. *The journal of histochemistry and cytochemistry : official journal of the Histochemistry Society* 57, 249-256 (2009).

30. V. Tam *et al.*, Histological and reference system for the analysis of mouse intervertebral disc. *J Orthop Res* 36, 233-243 (2018).

31. M. B. Delisle, M. Laroche, H. Dupont, P. Rochaix, J. L. Rumeau, Morphological analyses of paraspinal muscles: comparison of progressive lumbar kyphosis (camptocormia) and narrowing of lumbar canal by disc protrusions. *Neuromuscul Disord* 3, 579-582 (1993).

32. H. W. D. Hey, K. A. Tan, B. Z. Chin, G. Liu, H. K. Wong, Comparison of whole body sagittal alignment during directed vs natural, relaxed standing postures in young, healthy adults. *The spine journal : official journal of the North American Spine Society* 19, 1832-1839 (2019).

33. D. Sun *et al.*, Correlation between intervertebral disc degeneration, paraspinal muscle atrophy, and lumbar facet joints degeneration in patients with lumbar disc herniation. *BMC musculoskeletal disorders* 18, 167 (2017).

34. A. J. Teichtahl *et al.*, Lumbar disc degeneration is associated with modic change and high paraspinal fat content - a 3.0T magnetic resonance imaging study. *BMC musculoskeletal disorders* 17, 439 (2016).

Thoracic Kyphosis in Women and Men: The Framingham Study. *The journals of gerontology. Series A, Biological sciences and medical sciences* 74, 420-427 (2019).

36. D. H. Kim, S. Y. Lee, S. J. Park, Y. S. Lee, Relationships between Spinal Sarcopenia and Spinal Sagittal Balance in Older Women. *Ann Geriatr Med Res* 23, 141-148 (2019).

37. W. Xia *et al.*, Association between back muscle degeneration and spinal-pelvic parameters in patients with degenerative spinal kyphosis. *BMC musculoskeletal disorders* 20, 454 (2019).

38. K. Iba *et al.*, Mice with a targeted deletion of the tetranectin gene exhibit a spinal deformity. *Molecular and cellular biology* 21, 7817-7825 (2001).

39. G. B. Andersson, R. Ortengren, A. Nachemson, Intradiskal pressure, intra-abdominal pressure and myoelectric back muscle activity related to posture and loading. *Clin Orthop Relat Res* 10.1097/00003086-197711000-00018, 156-164 (1977).

40. K. Sato, S. Kikuchi, T. Yonezawa, In Vivo Intradiscal Pressure Measurement in Healthy Individuals and in Patients With Ongoing Back Problems. *Spine* 24, 2468 (1999).

41. C. Neidlinger-Wilke *et al.*, Mechanical loading of the intervertebral disc: from the macroscopic to the cellular level. *Eur Spine J* 23 Suppl 3, S333-343 (2014).

42. J. C. Lotz, O. K. Colliou, J. R. Chin, N. A. Duncan, E. Liebenberg, Compression-induced degeneration of the intervertebral disc: an in vivo mouse model and finite-element study. *Spine* 23, 2493-2506 (1998).

43. S. K. Han *et al.*, In vivo study of paraspinal muscle weakness using botulinum toxin in one primate model. *Clinical biomechanics (Bristol, Avon)* 53, 1-6 (2018).

44. I. A. Stokes, J. C. Iatridis, Mechanical conditions that accelerate intervertebral disc degeneration: overload versus immobilization. *Spine* 29, 2724-2732 (2004).

45. H. T. Hee, H. D. Ismail, C. T. Lim, J. C. Goh, H. K. Wong, Effects of implantation of bone marrow mesenchymal stem cells, disc distraction and combined therapy on reversing degeneration of the intervertebral disc. *J Bone Joint Surg Br* 92, 726-736 (2010).

46. H. T. Hee, Y. J. Chuah, B. H. Tan, T. Setiobudi, H. K. Wong, Vascularization and morphological changes of the endplate after axial compression and distraction of the intervertebral disc. *Spine* 36, 505-511 (2011).

47. E. Montgomery, C. Pennington, C. M. Isales, M. W. Hamrick, Muscle-bone interactions in dystrophin-deficient and myostatin-deficient mice. *Anat Rec A Discov Mol Cell Evol Biol* 286, 814-822 (2005).

48. E. Behrbalk *et al.*, Staged Correction of Severe Thoracic Kyphosis in Patients with Multilevel Osteoporotic Vertebral Compression Fractures. *Global spine journal* 6, 710-720 (2016).

49. V. Glatt, E. Canalis, L. Stadmeyer, M. L. Bouxsein, Age-related changes in trabecular architecture differ in female and male C57BL/6J mice. *J Bone Miner Res* 22, 1197-1207 (2007).
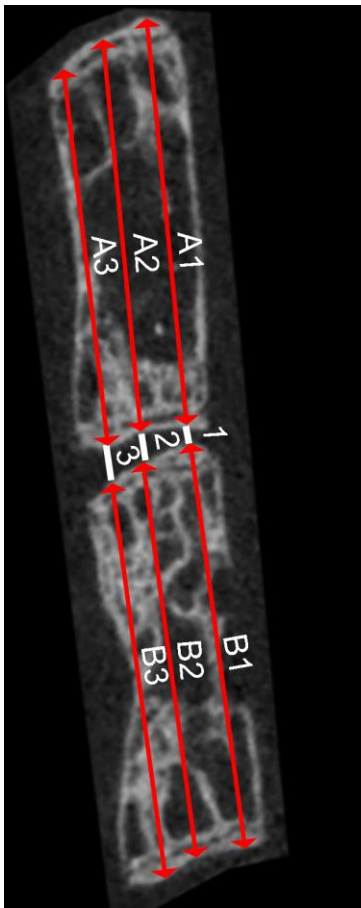
$$\text{Disc Height Index} = \frac{2\,(DH1 + DH2 + DH3)}{A1 + A2 + A3 + B1 + B2 + B3}$$

$$\text{Disc Wedge Index} = \frac{DH3}{DH1}$$

Figure 1. Diagram demonstrating the calculation for Disc Height Index (DHI) and Disc Wedge Index (DWI).
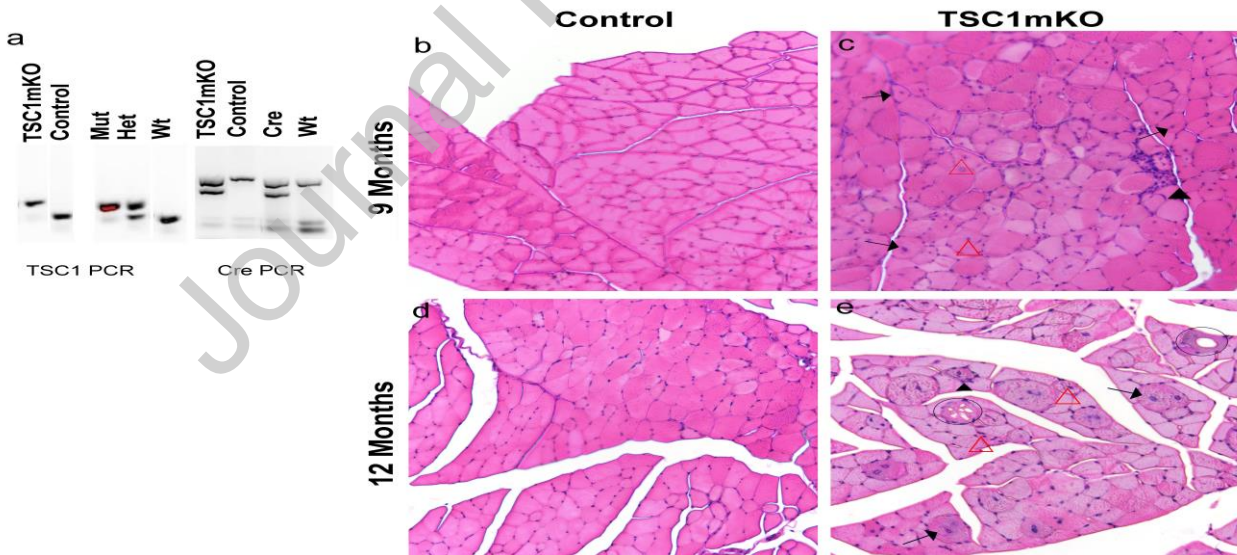

Figure 2. (a) PCR result of TSC1 and Cre gene. (B-E) H&E staining of paraspinal muscle in (b) 9-months-old control mice, (c) 9-months-old TSC1mKO mice, (d) 12-months-old control mice and (e) 12-months-old TSC1mKO mice. Figures b to e demonstrate increased presence of intracellular inclusions (black triangle), central nuclei (red triangle), large myonuclei (thin arrow) and vacuolated fibers (circle) in TSC1mKO mice, especially at 12 months old. Magnification 400X.
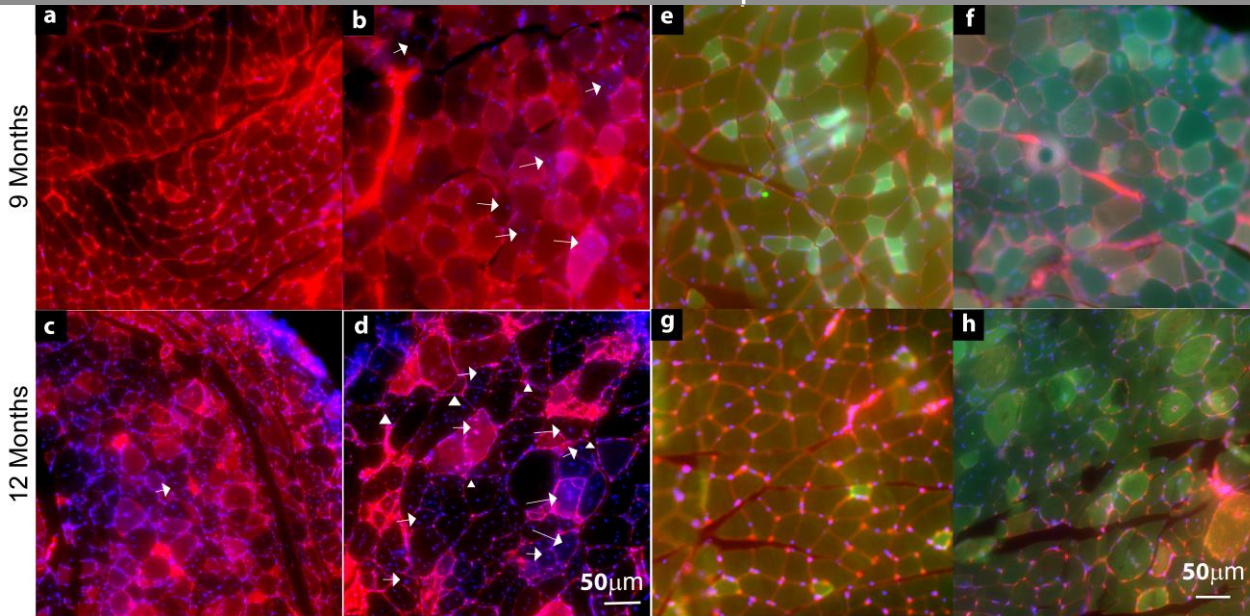
Figure 3. (a-d) WGA stained muscle fiber (Red) and DAPI stained nucleus (Blue) in (A) 9-months-old control mice, (b) 9-months-old TSC1mKO mice, (c) 12-months-old control mice and (d) 12-months-old TSC1mKO mice. Figures a to d demonstrate increased muscle fibre size, presence of small triangular fiber (White Triangle) and central nucleus (White Arrow) in TSC1mKO mice, especially at 12 months old. Magnification 200X, Scale Bar 50 μm. (e-h) Immunofluorescence stained muscle fibers in (e) 9 months old control mice, (f) 9 months old TSC1mKO mice, (g) 12 months old control mice and (h) 12 months old TSC1mKO mice. Figures e to h demonstrate higher percentage of PGC-1α-stained (Green) muscle fiber in 12 months old TSC1mKO mice. Magnification 200X, Scale Bar 50 μm.
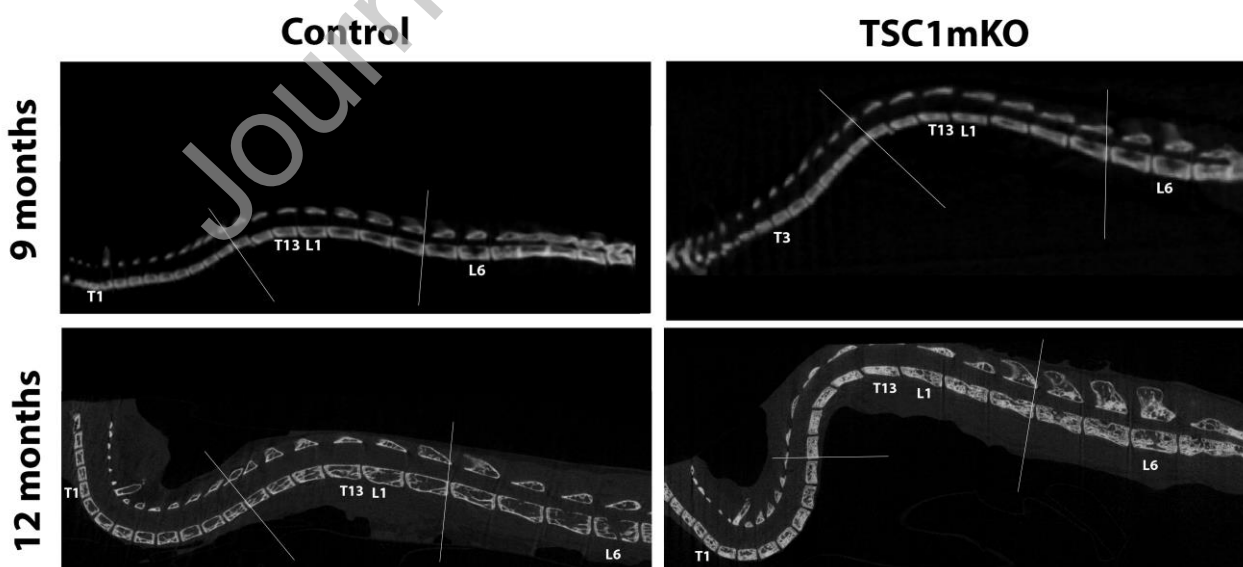
Figure 4. Micro-CT sagittal view of the spine in 9- and 12-months-old control and TSC1mKO mice demonstrating accelerated thoracolumbar kyphosis in TSC1mKO mice which increases with age.

22
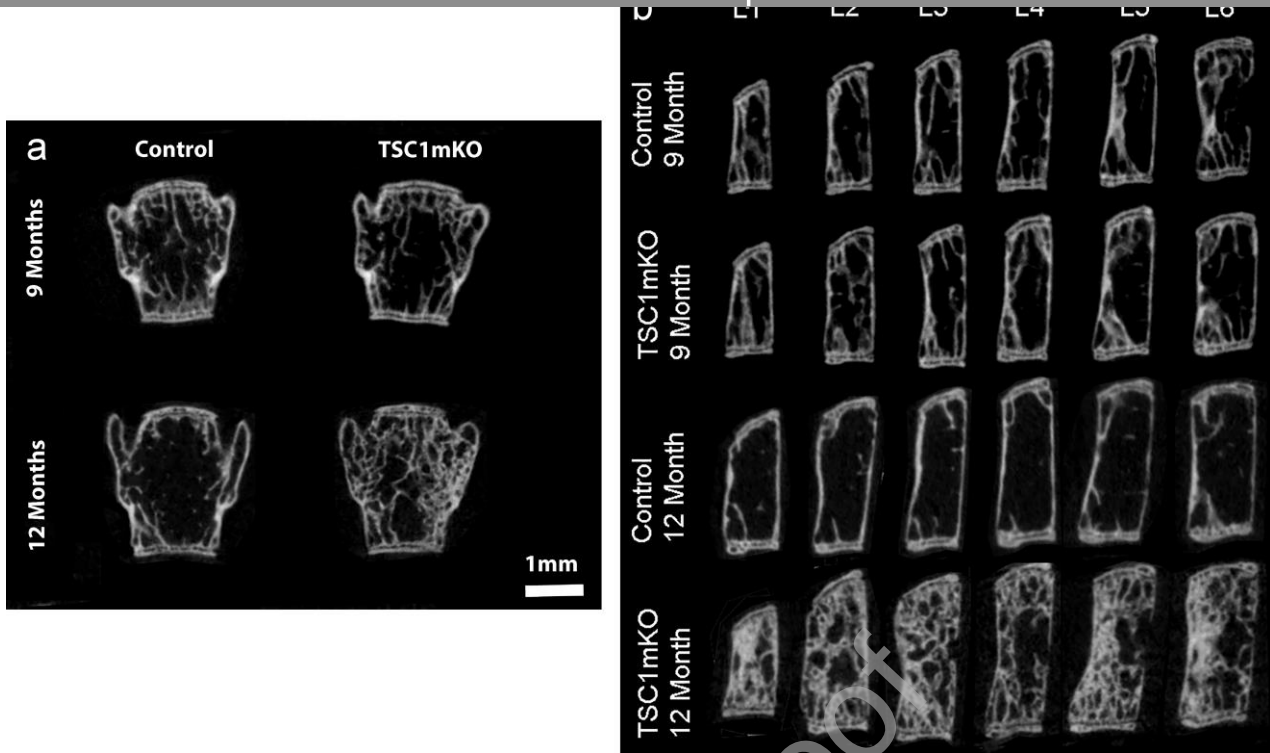
Figure 5. (a) Micro-CT coronal view of L5 vertebra in 9- and 12-months-old control and TSC1mKO mice showing higher bone volume fraction in TSC1mKO mice compared to controls. (b) Micro-CT Sagittal views of L1 to L6 vertebra in 9- and 12-months-old control and TSC1mKO mice higher vertebral body posterior to anterior ratio suggesting wedging in TSC1mKO mice which increases with age.

Figure 6. Sagittal FAST stained sections of L1/2 to L5/6 intervertebral disc in 9- and 12-months-old control and TSC1mKO mice showing progressive disc degeneration with age, more so at the lower lumbar levels in TSC1mKO mice. Disc degeneration is evidenced by reduction of extracellular matrix (blue), nucleus pulposus cells (orange halo) and widened annulus fibrosus lamellae (orange). Magnification 100X, scale bar 500 μm.

Table 1. Comparison of Cobb angle, vertebral height and trabecular bone histomorphometry findings in 9- and 12-months-old TSC1mKO and Control mice

	9 Months		12 Months		Comparison analysis (*P* value)			
	Control (n=4)	TSC1mKO (n=7)	Control (n=9)	TSC1mKO (n=8)	9 Months Control vs TSC1mKO	12 Months Control vs TSC1mKO	TSC1mKO 9 Months vs 12 Months	Control 9 Months vs 12 Months
Vertebra Height (µm, mean ± SD)								
L1	2774 ± 209	2710 ± 371	3041 ± 278	3127 ± 149	0.386	0.192	0.029*	0.104
L2	2988 ± 224	2915 ± 164	3169 ± 266	3301 ± 111	0.118	0.093	0.001*	0.254
L3	3155 ± 91	3044 ± 91	3271 ± 129	3371 ± 150	0.114	0.051	0.0002*	0.103
L4	3148 ± 142	2928 ± 199	3391 ± 145	3411 ± 103	0.096	0.295	0.001*	0.026*
L5	3028 ± 111	2842 ± 80	3351 ± 127	3397 ± 163	0.004*	0.213	<0.001*	0.001*
L6	2812 ± 143	2744 ± 178	3323 ± 145	3374 ± 173	0.197	0.267	0.0001*	0.006*
Vertebra Wedging (Posterior/Anterior Ratio, mean ± SD)								
L1	1.06 ± 0.04	1.11 ± 0.04	1.08 ± 0.02	1.11 ± 0.04	0.087	0.355	0.441	0.101
L2	1.07 ±	1.14 ±	1.09 ±	1.11 ±	0.035*	0.054	0.171	0.209

L3	1.03 ± 0.07	1.14 ± 0.04	1.06 ± 0.01	1.08 ± 0.03	0.040*	0.062	0.056	0.226
L4	1.06 ± 0.03	1.08 ± 0.04	1.05 ± 0.03	1.04 ± 0.04	0.337	0.400	0.167	0.267
L5	1.04 ± 0.02	1.07 ± 0.03	1.02 ± 0.01	1.03 ± 0.04	0.123	0.097	0.076	0.057
L6	1.03 ± 0.01	1.01 ± 0.02	1.02 ± 0.01	1.02 ± 0.02	0.119	0.446	0.351	0.046*
BV/TV (%, mean ± SD)							
L1	20.97 ± 5.51	29.50 ± 14.77	18.00 ± 7.88	33.08 ± 9.11	0.214	0.001*	0.362	0.252
L2	19.56 ± 7.53	22.94 ± 10.88	11.81 ± 3.91	33.25 ± 10.46	0.342	<0.001*	0.120	0.105
L3	17.18 ± 6.51	18.62 ± 7.32	12.38 ± 4.26	29.41 ± 11.67	0.406	0.002*	0.058	0.165
L4	16.48 ± 3.91	20.72 ± 9.58	10.27 ± 4.33	27.97 ± 9.13	0.268	<0.001*	0.165	0.042*
L5	18.20 ± 4.21	27.26 ± 9.54	12.48 ± 5.13	29.73 ± 10.55	0.119	0.001*	0.364	0.062
L6	15.04 ± 3.95	28.72 ± 15.10	13.53 ± 5.46	28.23 ± 4.51	0.127	<0.001*	0.480	0.347
Tb.Th (μm, mean ± SD)							
L1	75 ± 5	83 ± 10	82 ± 13	106 ± 10	0.124	<0.001*	0.018*	0.092
L2	77 ± 7	88 ± 24	80 ±	117 ± 11	0.210	<0.001*	0.083	0.219

L3	74 ± 8	83 ± 17	80 ± 7	109 ± 17	0.221	0.001*	0.043*	0.171
L4	79 ± 8	90 ± 20	78 ± 5	112 ± 21	0.228	0.001*	0.090	0.403
L5	86 ± 5	105 ± 20	83 ± 10	123 ± 24	0.108	0.001*	0.136	0.443
L6	80 ± 2	96 ± 23	85 ± 10	117 ± 13	0.124	<0.001*	0.018*	0.092
Tb.Sp (µm, mean ± SD)								
L1	255 ± 44	208 ± 14	286 ± 56	218 ± 38	0.098	0.005*	0.282	0.188
L2	280 ± 48	264 ± 70	372 ± 68	291 ± 212	0.376	0.164	0.380	0.002*
L3	279 ± 21	299 ± 29	406 ± 26	255 ± 63	0.192	<0.001*	0.076	<0.001*
L4	397 ± 21	358 ± 67	440 ± 95	291 ± 47	0.339	0.001*	0.106	0.042*
L5	407 ± 79	346 ± 80	471 ± 42	316 ± 59	0.200	<0.001*	0.300	0.072
L6	363 ± 79	319 ± 63	385 ± 65	296 ± 46	0.290	0.002*	0.302	0.461
Tb.N (mm^{-1}, mean ± SD)								
L1	2.41 ± 0.46	2.83 ± 0.25	2.41 ± 0.46	3.10 ± 0.73	0.128	0.008*	0.191	0.241
L	2.17 ±	2.13 ±	2.17 ±	2.87 ±	0.388	0.001*	0.030*	<0.001

L 3	1.93 ± 0.44	1.84 ± 0.32	1.93 ± 0.44	2.63 ± 0.72	0.393	0.002*	0.018*	0.134
L 4	1.82 ± 0.61	1.93 ± 0.74	1.82 ± 0.61	2.45 ± 0.50	0.425	<0.001*	0.174	0.149
L 5	1.84 ± 0.39	2.19 ± 0.53	1.84 ± 0.39	2.38 ± 0.59	0.206	0.003*	0.316	0.131
L 6	1.84 ± 0.47	2.39 ± 0.61	1.84 ± 0.47	2.43 ± 0.44	0.128	0.008*	0.191	0.241

* $p < 0.05$

Table 2. Summary of significant findings comparing 9- and 12-months-old TSC1mKO and

Control mice

Components	Features	In 9 Months TSC1mKO compared to Controls:	In 12 Months TSC1mKO compared to Controls:
Muscle	Features of myopathy	+	++
	Greater density of small triangular fibre	+	+
	Greater density of central nucleus	+	+
	Larger muscle fibre size	-	+
	Greater erector spinae muscle cross-sectional area	-	+
	Greater density of PGC-1α stained fibre	-	-
Spinal alignment	Greater cobb angle	-	+
Bone	Higher bone volume fraction in Coronal sections of L5 vertebra	+	++
	Higher bone sclerosis at anterior aspect of vertebral body	-	+
	Higher bone volume fraction (BV/TV)	-	+
	Higher trabecular number (Tb.N)	-	+
	Higher trabecular thickness (Tb.Th)	-	+
	Lower trabecular separation (Tb.Sp)	-	+
	Loss of vertebral height	-	-
	Higher vertebral body posterior/anterior ratio	-	-

29

Disc	Features of disc degeneration	+	++
	Higher disc scores	+	+
	Higher disc wedge index	+	++
	Lower disc height index	-	++

+ present; - absent